

A synthetic electric force acting on neutral atoms

Y.-J. Lin¹, R. L. Compton¹, K. Jiménez-García^{1,2}, W. D. Phillips¹, J. V. Porto¹, and I. B. Spielman¹

¹*Joint Quantum Institute, National Institute of Standards and Technology,
and University of Maryland, Gaithersburg, Maryland, 20899, USA and*

²*Departamento de Física, Centro de Investigación y Estudios Avanzados
del Instituto Politécnico Nacional, México D.F., 07360, México*

(Dated: February 23, 2024)

Electromagnetism is a simple example of a gauge theory where the underlying potentials – the vector and scalar potentials – are defined only up to a gauge choice. The vector potential generates magnetic fields through its spatial variation and electric fields through its time-dependence. We experimentally produce a synthetic gauge field that emerges only at low energy in a rubidium Bose-Einstein condensate: the neutral atoms behave as charged particles do in the presence of a homogeneous effective vector potential. We have generated a synthetic electric field through the time dependence of an effective vector potential, a physical consequence even though the vector potential is spatially uniform.

Gauge theories play a central role in modern quantum physics. In some cases, they can be viewed as emerging as the low energy description of a more complete theory [1, 2]. Electromagnetism is the best known gauge theory and its gauge fields are the ordinary scalar and vector potentials. Magnetic fields arise only from spatial variations (curl) of the vector potential, while electric fields arise from both time variations of the vector potential and gradients of the scalar potential; these potentials are defined only to within a gauge choice. For a charged particle in such potentials the canonical momentum (the variable canonically conjugate to position) and the mechanical momentum (mass times the velocity) are not equal. Our experiments [3] have realized a particular version [4] of a class of proposals [5–10] to generate effective vector potentials for neutral atoms via interactions with laser light, and have created synthetic magnetic fields [11] on the success of simulating charged condensed matter systems with neutral atoms [12, 13]. Here we demonstrate the complementary phenomenon: the generation of a synthetic electric field from a time-dependent effective vector potential. Additionally, we make independent measurements of both the mechanical momentum and canonical momentum, where the latter is usually not possible.

Introduction The electromagnetic vector potential \mathbf{A} for a charged particle appears in the Hamiltonian $H = (\mathbf{p}_{\text{can}} - q\mathbf{A})^2/2m$, where \mathbf{p}_{can} is the canonical momentum, q is the charge, and m is the mass. (The quantity $\mathbf{p}_{\text{can}} - q\mathbf{A} = m\mathbf{v}$ is the mechanical momentum for a particle moving with velocity \mathbf{v} .) We recently demonstrated a technique to engineer Hamiltonians of this form for ultra-cold atoms, and prepared a Bose-Einstein condensate (BEC) at rest with an effective vector potential $\mathbf{A}_0 = A_x \hat{x}$ constant in time and space [3], corresponding to $\mathbf{E} = \mathbf{B} = 0$. In Ref. [11], we made \mathbf{A} depend on position giving $\mathbf{B} = \nabla \times \mathbf{A} \neq 0$ but $\mathbf{E} = 0$. Here we add time dependence to a spatially uniform vector potential $\mathbf{A}(t) = A(t)\hat{x}$, generating a synthetic electric field $E(t)\hat{x} = -\partial\mathbf{A}/\partial t$. The resulting force is distinct from that due to fields arising from gradients of scalar

potentials $\phi(\mathbf{r})$ like gravity or an external trapping potential. A revealing analog to which we will return is that of an infinite solenoid of radius r_0 as pictured in Fig. 1A: a magnetic field $\mathbf{B} = B\hat{z}$ exists only inside the coil, however, a non-zero cylindrically symmetric vector potential $\mathbf{A} = Br_0^2\hat{\phi}/2r$ in the symmetric gauge extends outside the coil. Far from the coil, \mathbf{A} is nearly uniform, analogous to our uniform effective vector potential.

We experimentally synthesize electromagnetic fields for neutral atoms by illuminating an atomic ^{87}Rb BEC with two intersecting laser beams (Fig. 2A) that couple together three atomic spin states within the $5S$ electronic ground state. The three new energy eigenstates, or “dressed states,” are superpositions of the uncoupled spin and linear-momentum states and have energy-momentum dispersion relations that can be dramatically different from those of uncoupled atoms. The atoms in a dressed state act as particles with a single well-defined velocity \mathbf{v} , which is the population-weighted average of all three spin components.

The dispersion relation of the lowest energy dressed state changes near its minimum, from $\mathbf{p}^2/2m$ to $(\mathbf{p} - \mathbf{p}_{\text{min}})^2/2m^*$ (as shown in Fig. 2C), where the minimum location \mathbf{p}_{min} plays the role of $q\mathbf{A}$. In addition, the mass m is modified to an effective mass m^* , $m^* > m$, and both \mathbf{p}_{min} and m^* are under experimental control (although not completely independently). We identify $\mathbf{p}_{\text{min}} = q^*\mathbf{A}^*$, the product of an effective charge q^* and an effective vector potential \mathbf{A}^* for the dressed neutral atoms. As we change \mathbf{A}^* in time, we induce a synthetic electric field $\mathbf{E}^* = -\partial\mathbf{A}^*/\partial t$, and the dressed BEC responds as $d(m^*\mathbf{v})/dt = -\nabla\phi(\mathbf{r}) + q^*\mathbf{E}^*$, where \mathbf{v} is the velocity of the dressed atoms and $m^*\mathbf{v} = \mathbf{p}_{\text{can}} - q^*\mathbf{A}^*$. Here, $\Delta(m^*\mathbf{v}) = -q^*(\mathbf{A}_f^* - \mathbf{A}_i^*)$ is the momentum impulse imparted by the synthetic electric force $q^*\mathbf{E}^*$.

We study the physical consequences of sudden temporal changes of the effective vector potential for the dressed BEC. These changes are always adiabatic such that the BEC remains in the same dressed state. We measure the resulting change of the BEC’s momentum, which is in complete quantitative agreement with our calculations

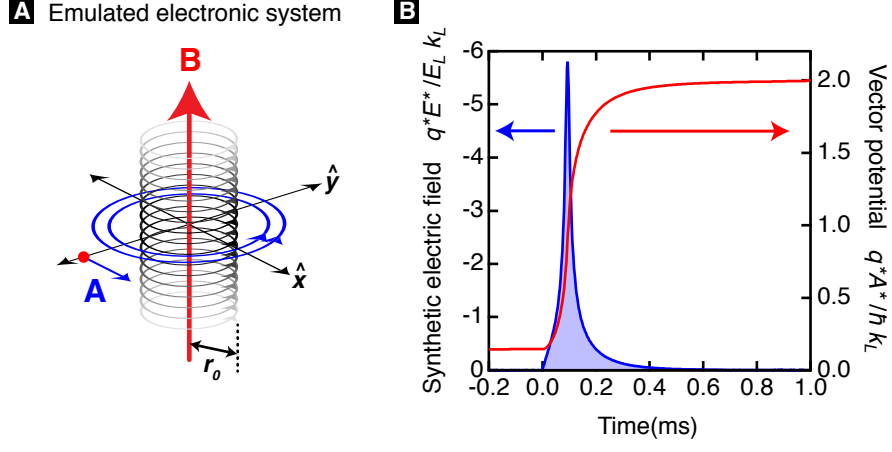


FIG. 1. Schematic of the electric field generated by a time varying vector potential. (A) Emulated system, showing the electric current flowing counter clockwise in the infinite solenoid (black coil) with radius r_0 and the real magnetic field \mathbf{B} only inside the solenoid. The blue lines represent the vector potential \mathbf{A} . A charged particle (red dot) located far from the coil experiences a nearly uniform \mathbf{A} . (B) Calculated time response of the synthetic vector potential and electric field for neutral atoms in our first measurement (see Fig. 3). The calculation includes the known inductive response time of the bias field B_0 , which sets the detuning, and the calibration of detuning to vector potential shown in Fig. 2D.

and constitutes the first observation of synthetic electric fields for neutral atoms.

Experimental realization Our system, depicted in Fig. 2A, consists of a $F = 1$ ^{87}Rb BEC with about 1.4×10^5 atoms initially at rest [14, 15]; a small physical magnetic field B_0 Zeeman-shifts each of the three magnetic sublevels $m_F = 0, \pm 1$ by an amount $E_{0,\pm 1}$, but produces no Lorentz force on our charge-neutral BEC. Our experiment is performed in the linear Zeeman regime, i.e., $E_{-1} \approx -E_{+1} \approx g\mu_B B_0 \gg |E_0|$, with linear and quadratic Zeeman shifts $\hbar\omega_Z = (E_{-1} - E_{+1})/2 \approx h \times 2.32$ MHz and $-\hbar\epsilon = E_0 - (E_{-1} + E_{+1})/2 \approx -h \times 784$ Hz. In addition, a pair of $\lambda = 801$ nm laser beams, intersecting at 90° at the BEC, couples the m_F states with strength Ω_R . These Raman lasers differ in frequency by $\Delta\omega_L \approx \omega_Z$ and we define the detuning from Raman resonance as $\delta = \Delta\omega_L - \omega_Z$. In our experiments $\hbar\Omega_R \approx 10E_L$ and $|\hbar\delta| < 60E_L$, where $E_L = \hbar^2 k_L^2 / 2m$ and $k_L = \sqrt{2\pi}/\lambda$ are the appropriate units of energy and momentum.

When the atoms are rapidly moving or the Raman lasers are far from resonance ($k_L v$ or $\delta \gg \Omega_R$), the coupling lasers hardly affect the atoms. However, nearly resonant, slowly moving atoms are strongly dressed: the three uncoupled states transform into three new dressed states. The spin and linear-momentum state $|k_x, m_F = 0\rangle$ is coupled to states $|k_x - 2k_L, m_F = +1\rangle$ and $|k_x + 2k_L, m_F = -1\rangle$, where $\hbar k_x$ is the momentum of $|m_F = 0\rangle$ along \hat{x} , and $2\hbar k_L \hat{x}$ is the momentum difference between two Raman beams. In the frame rotating at $\Delta\omega_L$ under the rotating wave approximation, the Hamiltonian matrix $H(k_x)/\hbar$ for motion along \hat{x} is

$$\begin{pmatrix} \frac{\hbar}{2m}(k_x + 2k_L)^2 - \delta & \Omega_R/2 & 0 \\ \Omega_R/2 & \frac{\hbar}{2m}k_x^2 - \epsilon & \Omega_R/2 \\ 0 & \Omega_R/2 & \frac{\hbar}{2m}(k_x - 2k_L)^2 + \delta \end{pmatrix}.$$

Diagonalization for each k_x yields three dressed eigenstates, each of which is a superposition of the uncoupled states [3], with energies $E_j(k_x)$ shown in Fig. 2C (gray for uncoupled states, colored for dressed states); we focus on atoms in the lowest energy energy-momentum (red) curve. When the atoms' energy (interaction and kinetic) is small compared to the $\approx 10E_L$ energy difference between the curves—as it is in our experiments—the contact-interacting atoms will remain within the lowest energy dressed state [4]. Such low energy particles do not reveal their spin and momentum components. In the low energy limit, dressed atoms have a new effective Hamiltonian for motion along \hat{x} , $H_x = (\hbar k_x - q^* A_x^*)^2 / 2m^*$ (motion along \hat{y} and \hat{z} is unaffected), where we have chosen a gauge such that the momentum of the $m_F = 0$ component $\hbar k_x \equiv p_{\text{can}}$ is the canonical momentum of the dressed state. Our approach introduces the term $q^* A_x^*$, which depends on the detuning δ as shown in Fig. 2D, and an effective mass m^* . The red curve in Fig. 2C shows H_x for $q^* A_x^* > 0$ and the arrow indicates the canonical momentum of a BEC in the lowest energy dressed state, $p_{\text{can}} = q^* A_x^*$. Although this dressed BEC is at rest ($v = \partial H_x / \partial \hbar k_x = 0$, zero group velocity), it is composed of three bare spin states each with a different momentum, among which the momentum of $|m_F = 0\rangle$ is $\hbar k_x = p_{\text{can}}$. Although none of its three bare spin components has zero momentum, the BEC's averaged momentum is zero.

We measure p_{can} by first removing the coupling fields and trapping potentials and then allowing the atoms to

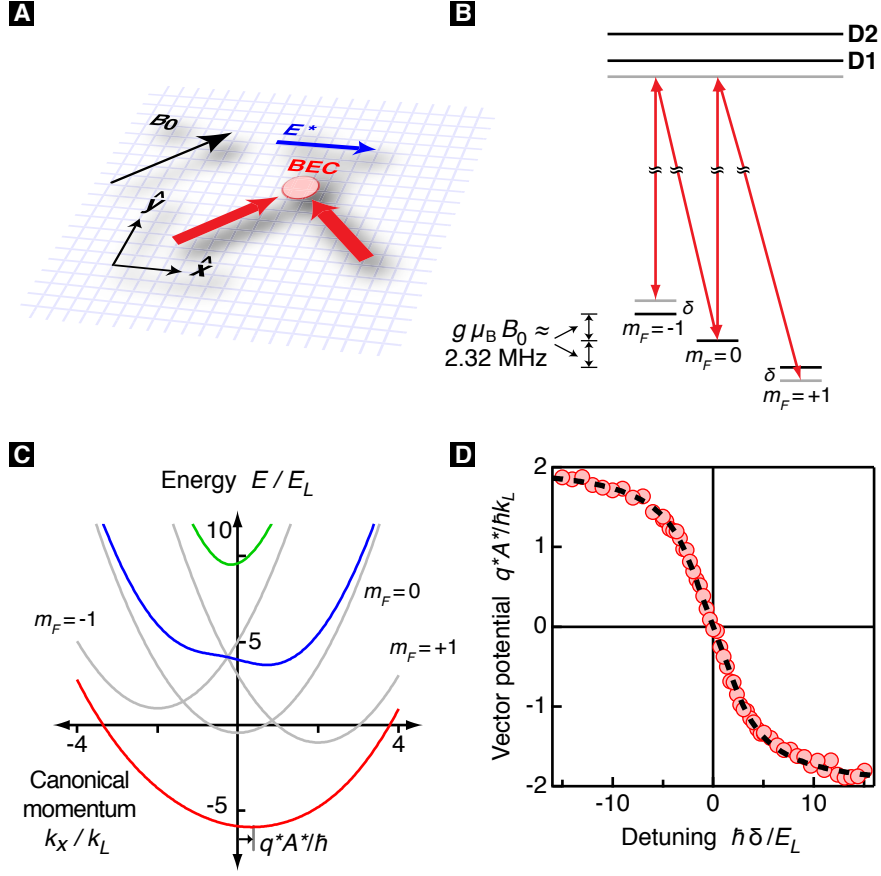


FIG. 2. Experiment setup for synthetic electric fields. (A) Physical implementation indicating the two Raman laser beams incident on the BEC (red arrows) and the physical bias magnetic field B_0 (black arrow). The blue arrow indicates the direction of the synthetic electric field E^* . (B) The three m_F levels of the $F = 1$ ground state manifold are shown as coupled by the Raman beams. (C) The dressed state eigenenergies as a function of canonical momentum for the realized coupling strength of $\hbar\Omega_R = 10.5E_L$ at a representative detuning $\hbar\delta = -1E_L$ (colored curves). The grey curves show the energies of the uncoupled states, and the red curve depicts the lowest energy dressed state in which we load the BEC. The black arrow indicates the dressed BEC's canonical momentum $p_{\text{can}} = q^*A^*$, where A^* is the vector potential. (D) Measured vector potential from the canonical momentum.

freely expand for a $t = 20.1$ ms time-of-flight (TOF). Because the three components of the dressed state $\{|k_x, m_F = 0\rangle, |k_x \mp 2k_L, m_F = \pm 1\rangle\}$ differ in momentum by $\pm\hbar 2k_L$, they quickly separate.

Using a combination of adiabatically applied Raman and rf (radio-frequency) fields we transfer (load) the BEC initially in $|m_F = -1\rangle$ into the lowest energy dressed state with a $\mathbf{A}^* = A^*\hat{x}$ (see Ref. [3] for a complete technical discussion of loading), i.e., with a canonical momentum $p_{\text{can}} = q^*A^*$. We measure q^*A^* as the momentum of $|m_F = 0\rangle$; Fig. 2D shows how the measured and predicted A^* depend on the detuning δ . With this calibration, we use δ to control the effective vector potential.

Synthetic electric field Electric fields result either from spatially varying scalar potentials or from time varying vector potentials. An example of the latter case is illustrated in Fig. 1A for an infinite solenoid. The magnetic field \mathbf{B} exits only inside the coil; when the cur-

rent is constant the electric field \mathbf{E} is everywhere zero but the symmetric gauge vector potential is zero only at the solenoid center. When the current is changed in a time interval Δt the magnetic field inside the coil changes to a final value $B(\Delta t)$, and the exterior vector potential changes by $\Delta\mathbf{A} = [B(\Delta t) - B(0)] r_0^2 \hat{\phi} / 2r$. Here, a charged particle on the \hat{y} axis feels an electric field $-(\partial A / \partial t)\hat{x}$ during the time Δt , leading to a mechanical momentum kick $\Delta\mathbf{p} = -q\Delta A\hat{x}$, even outside the solenoid.

We realize a synthetic electric field E^* for ultracold neutral atoms by changing the effective vector potential from an initial value A_i^* to a final value A_f^* . We perform two types of measurements of E^* : (1) we remove the trapping potential right before we change A^* such that E^* can accelerate the atoms unimpeded, and measure the resulting change from zero of the BEC's velocity; and (2) after changing A^* , we allow the trapped, dressed atoms

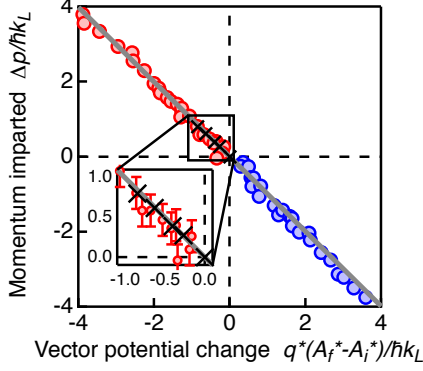


FIG. 3. Change in momentum from the synthetic electric field kick. This figure displays three distinct sets of data shown by red and blue circles and black crosses. The data were obtained by applying a synthetic electric field by changing the vector potential from $q^*A_i^*$ (between $+2\hbar k_L$ and $-2\hbar k_L$) to $q^*A_f^*$. Circles indicate data where the external trap was removed right before the change in A^* : for red (blue) symbols $q^*A_f^* = -2\hbar k_L$ ($+2\hbar k_L$). The black crosses, more visible in the inset, show the amplitude of canonical momentum oscillations when the trapping potential was left on after the field-kick. The typical uncertainties are also visible in the inset. The grey line is a linear fit to the data (circles) yielding slope -0.996 ± 0.008 , where the expected slope is -1 .

to oscillate in their harmonic potential, and measure the magnitude and frequency of the oscillations of both the canonical momentum and velocity.

We prepare our BEC at rest with an initial vector potential $A_i^*\hat{x}$. In the first measurement, we change the detuning δ in 0.8 ms, leading to a change of the vector potential to A_f^* , after which the Raman coupling is turned off in 0.2 ms. As A^* changes from A_i^* to A_f^* , a synthetic electric field E^* appears and accelerates the BEC. We image the atoms after a TOF and record their final velocities. Figure 3 shows the momentum Δp imparted to the atoms by E^* as a function of the vector potential change $q^*(A_f^* - A_i^*)$, denoted by red (blue) symbols with $q^*A_f^*/\hbar = 2k_L$ ($-2k_L$). We have chosen a sufficiently large final detuning $\hbar\delta = \mp 60E_L$ such that the final atomic state is a nearly pure spin state, $|m_F = +1\rangle$ for $q^*A_f^*/\hbar = 2k_L$ or $|m_F = -1\rangle$ for $q^*A_f^*/\hbar = -2k_L$. For this essentially undressed final state, $m^* = m$ and the imparted momentum is $\Delta p = m^*v = mv$, equal to the change in mechanical momentum. We performed a linear fit $\Delta p = Cq^*(A_f^* - A_i^*)$ to the data and obtain $C = -0.996(8)$, in good agreement with the expected $\Delta p = -q^*(A_f^* - A_i^*)$.

In the measurement described above, the final value of $A^* = A_f^*$ resulted from a detuning so large that the final-state atoms were essentially undressed. In a second measurement, we examined the time evolution of atoms that remain trapped and strongly dressed. Here we again

changed A^* from A_i^* to A_f^* in about $\Delta t = 0.3$ ms but left the dressed BEC in the harmonic confining potential for a variable time before abruptly removing the confining potential and the Raman fields for a TOF. As the BEC oscillated in the trap, we monitored the out-of-equilibrium canonical momentum p_{can} . It is our access to the internal degrees of freedom – here projectively measuring the composition of the Raman dressed state – that allows the determination of p_{can} . Figure 4A shows the resulting time evolution of p_{can} for several different initial A_i^* all for $A_f^* \approx 0$; as expected, we observe oscillations of p_{can} about $q^*A_f^*$. Since Δt is small compared to our ≈ 25 ms trap period, we expect the change of momentum to be dominated by $\Delta p = -q^*(A_f^* - A_i^*)$, where the contribution from the trapping force as A^* changes is negligible. This translates into an oscillation amplitude Δp in both p_{can} and $m^*v = p_{\text{can}} - q^*A_f^*$ of dressed atoms; the solid crosses in Fig. 3 show the amplitude of the sinusoidal oscillations in p_{can} as a function of $A_f^* - A_i^* \approx -A_i^*$, proving that the synthetic electric field has imparted the expected momentum kick.

We repeated the experiment with a nonzero $q^*A_f^*/\hbar \approx 0.35k_L$, and observed, remarkably, the sinusoidal oscillations in p_{can} were offset from zero as depicted in Fig. 4B. p_{can} evolves smoothly about $q^*A_f^* \neq 0$, illustrating the observed quantity is not the mechanical momentum mv , which should oscillate about zero. We also measured mv , where v is the population-weighted average velocity of all spin components; while mv indeed oscillates about zero, the oscillation amplitude is smaller than that of p_{can} . Given an increased effective mass $m/m^* \approx 0.4$, the trap frequency ν_x along \hat{x} was reduced by $\sqrt{m/m^*}$ from that for undressed atoms, and the oscillation amplitude of mv should be reduced by m/m^* from that of p_{can} . Our results show a reduction factor of $0.38(4)$ in ν_x^2 , in agreement with the predicted m/m^* , and the reduction factor of $0.30(2)$ in the momentum oscillation amplitude is slightly smaller than predicted.

Conclusion We have demonstrated how a time-dependent, spatially uniform effective vector potential for low-energy dressed neutral atoms gives rise to a synthetic electric force. We have measured the effect of such forces for both trapped and untrapped atoms, and for the final state both dressed and undressed. While the electric forces generated here are spatially homogenous, this technique is generally applicable to create spatially varying forces. Indeed, since the effective vector potential A^* is parameterized by the Raman detuning δ , it can be locally patterned via suitable spatially inhomogeneous magnetic fields or vector light shifts, giving rise to a nearly arbitrary range of time-dependent potentials. For azimuthal vector potentials, our method of measuring both the mechanical and canonical momentum from the induced electric fields can be used to identify the superfluid fraction of a BEC [16], or any other cold-atom systems.

This work was partially supported by ONR, ARO with funds from the DARPA OLE program, and the NSF

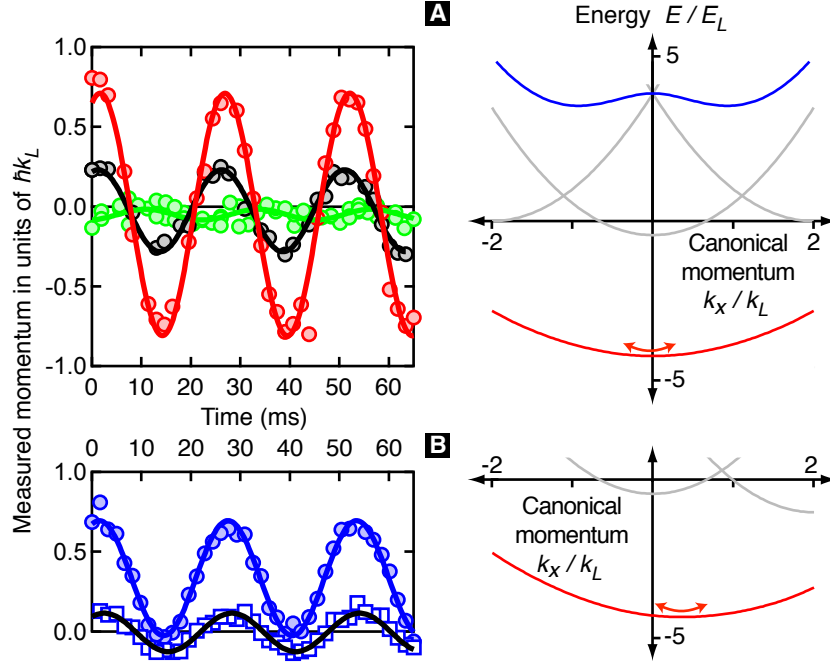


FIG. 4. Oscillating atoms in the trapping potential after application of a synthetic electric field pulse. (A)(B) Left panels: The vector potential is changed from $q^*A_i^* = 0.75 \hbar k_L$ (red circles), $0.25 \hbar k_L$ (black circles), and $q^*A_i^* = q^*A_f^* \approx 0$ (green circles), respectively, all to $q^*A_f^*$, and from $q^*A_i^* = 0.75 \hbar k_L$ (blue circles) to $q^*A_f^* = 0.35 \hbar k_L$ (blue squares). The measured momentum for all circles is the canonical momentum p_{can} , and that for the square is the mechanical momentum mv . In (B), p_{can} oscillates about $q^*A_f^* \neq 0$ while mv oscillates about zero. Right panels: Energy-momentum dispersion curves for uncoupled states (grey) and dressed states (colored). The arrows indicate oscillations of p_{can} about $q^*A_f^*$ for atoms in the lowest energy dressed state.

through the JQI Physics Frontier Center. R.L.C. ac-

knowledges the NIST/NRC postdoctoral program and K.J.-G thanks CONACYT.

-
- [1] M. Levin and X.-G. Wen, Rev. Mod. Phys. **77**, 871 (2005).
 [2] B. L. Hu, J. Phys. Conf. Ser. **174**, 012015 (2009).
 [3] Y.-J. Lin, R. L. Compton, A. R. Perry, W. D. Phillips, J. V. Porto, and I. B. Spielman, Phys. Rev. Lett. **102**, 130401 (2009).
 [4] I. B. Spielman, Phys. Rev. A **79**, 063613 (2009).
 [5] G. Juzeliūnas, J. Ruseckas, P. Öhberg, and M. Fleischhauer, Phys. Rev. A **73**, 025602 (2006).
 [6] K. J. Günter, M. Cheneau, T. Yefsah, S. P. Rath, and J. Dalibard, Phys. Rev. A **79**, 011604 (2009).
 [7] M. Cheneau, S. P. Rath, T. Yefsah, K. J. Gunter, G. Juzeliūnas, and J. Dalibard, Europhys. Lett. **83**, 60001 (6pp) (2008).
 [8] F. Gerbier and J. Dalibard, New Journal of Physics **12**, 033007 (2010).
 [9] G. Juzeliūnas, J. Ruseckas, and J. Dalibard, Phys. Rev. A **81**, 053403 (2010).
 [10] J. Ruseckas, G. Juzeliūnas, P. Ohberg, and M. Fleischhauer, Phys. Rev. Lett. **95** (2005).
 [11] Y.-J. Lin, R. L. Compton, K. Jimenez-Garcia, J. V. Porto, and I. B. Spielman, Nature **462**, 628 (2009).
 [12] N. R. Cooper, Adv. Phys. **57**, 539 (2008).
 [13] I. Bloch, J. Dalibard, and W. Zwerger, Rev. Mod. Phys. **80**, 885 (2008).
 [14] Y.-J. Lin, A. R. Perry, R. L. Compton, I. B. Spielman, and J. V. Porto, Phys. Rev. A **79**, 063631 (2009).
 [15] C.-L. Hung, X. Zhang, N. Gemelke, and C. Chin, Phys. Rev. A **78**, 011604 (2008).
 [16] N. R. Cooper and Z. Hadzibabic, Phys. Rev. Lett. **104**, 030401 (2010).
 [17] Y. Castin and R. Dum, Phys. Rev. Lett. **77**, 5315 (1996).

METHODS

1 Dynamic change of effective vector potentials

In our first measurement of synthetic electric fields, we observed the momentum imparted by the field kick, resulting from a change in the effective vector potential

from an arbitrarily chosen $q^*A_i^*$ to $q^*A_f^* = \pm 2\hbar k_L$ (see Fig. 3). In principle we could use any A_f^* and observe a momentum kick $q^*(A_i^* - A_f^*)$, however, in general the effective vector potential also depends on the strength of the Raman coupling Ω_R . As a result, additional synthetic electric fields typically appear when Ω_R is adiabatically turned off. There are three specific cases for which A^* does not depend on Ω_R : when the detuning $\delta = 0$ and $\delta \rightarrow \pm\infty$. For the former case, only when $|q^*A_i^*| < \hbar k_L$ is there no additional electric force during the removal of Ω_R , where the final atomic state is $|m_F = 0\rangle$. For $|q^*A_i^*| > \hbar k_L$, the final atomic state is $|m_F = \pm 1\rangle$ with an additional momentum of $\mp 2\hbar k_L$ imparted. Thus in our experiment we changed the vector potential from $q^*A_i^*$ to $q^*A_f^* = \pm 2\hbar k_L$ by changing the detuning from δ_i to a large $\hbar\delta_f = \mp 60E_L$; the subsequent turnoff of Ω_R then exerted no additional forces.

2 Control of Raman detuning

In all of our experiments, we set the Raman detuning δ with small changes of the bias magnetic field away from resonance and hold the 2.32 MHz frequency difference between the Raman beams constant. Because all temporal changes in δ lead to synthetic electric fields, bias magnetic field noise and relative laser frequency noise can lead to motion in the trap or heating. We phase locked the two Raman beams and observed no change in the heating, showing that relative laser frequency noise is not important in our experiment. However, our exper-

iment is very sensitive to ambient magnetic field noise, here tied to the 60 Hz line. This noise gives rise to intractable dynamics of the canonical momentum of the dressed state, where δ is held constant after the loading. We measured the field noise from the state-decomposition of a rf-dressed state (no Raman fields) nominally on resonance and then feed-forward canceled the field noise. This reduced the $\sim 0.2 \mu\text{T}$ RMS magnetic field noise at 60 Hz by about a factor of 20, and remaining RMS field noise is $\sim 0.03 \mu\text{T}$ (including all frequency components up to $\approx 5 \text{ kHz}$). All of our measurements were performed by locking to the 60 Hz line before loading into the dressed state.

3 Momentum measurements of the dressed state

The Raman-dressed state (no rf) is a superposition of spin and momentum components; its canonical momentum p_{can} is the momentum of the spin $m_F = 0$ component. Experimentally, we fit the $m_F = 0$ density distribution after TOF to a Thomas-Fermi profile[17] and identify p_{can} as the center of the distribution. The mechanical momentum of the dressed state mv was measured by a population-weighted average over all three spin states including every pixel with discernable atoms in the image. This takes into account the modification of the TOF density distribution for all m_F states due to interactions during TOF. Although interactions can exchange momentum between spin states, the total momentum is conserved.